Hypervelocity Impact Testing of a Metallic Glass-Stuffed Whipple Shield**

Douglas C. Hofmann[1 *], Lee Hamill[2], Eric Christiansen[3], Steve Nutt[2]

1. California Institute of Technology Keck Laboratory of Engineering Sciences Pasadena CA USA
2. University of Southern California Los Angeles CA USA
3. NASA Johnson Space Center Houston TX USA

Abstract: In this work, hypervelocity impact tests up to 7 km s^{-1} are used to compare the performance of Whipple shields integrated with layers of metallic glasses with a baseline target analogue of one of the shields similar to what is used on the International Space Station. The baseline target failed under the impact while the target utilizing metallic glass as a replacement for the fabric layers in the baseline passed the test. The paper postulates on the prospects of future implementation of metallic glasses as spacecraft debris shields.

*Jet Propulsion Laboratory, California Institute of Technology, Pasadena, CA, USA

**Part of this research was carried out at the Jet Propulsion Laboratory, California Institute of Technology, under a contract with the National Aeronautics and Space Administration. This work was funded by the Office of Air Force Research under grant number FA9550–12-1–0059_5 and NASA's Exploration Systems Mission Directorate under Contract No. MSFC-NRA10. The authors thank the staff of the White Sands Test Facility for their assistance with the tests and A. Kunz for sample preparation

1. Introduction

Low-Earth orbiting spacecraft and satellites are in constant threat of collision from an ever-increasing flux of hypervelocity particles [1–4]. Impacts of this nature were recognized early on in the space program and much effort has been devoted to developing shielding materials and geometries that can best mitigate these threats while maintaining the low-areal density required for

"Hypervelocity Impact Testing of a Metallic Glass-Stuffed Whipple Shield" DC Hofmann, L Hamill, E Christianson, and S Nutt, Adv Engrg Matls (2015) 1-10 DOI<http://dx.doi.org/10.1002/adem.201400518>

space applications. Research during the 1950–1970s demonstrated that multi-walled shields, subsequently termed “Whipple shields,” were effective at vaporizing and diffusing the debris associated with small projectile impacts [1]. These shields have found widespread use on spacecraft, satellites, and the International Space Station (ISS) [1–8]. A common Whipple-type shield is comprised of three layers separated by a gap, called standoff. The outer layer, termed the “bumper,” primarily functions by vaporizing an incident projectile and is usually comprised of a thin panel of aluminum. The intermediate layers are typically a high-strength cloth and the last layer is usually the wall of the spacecraft. Whipple shields operate effectively against projectile impacts; however with increasing worldwide space activity, the amount of man-made space debris is increasing at a near exponential rate. Spacecraft and satellites traveling through this flux of debris and micrometeoroids are increasingly likely to experience an impact, which puts a higher demand on the performance of the shields [1]. As the risk-posture for missions must now incorporate this larger threat, substantial research efforts have been devoted to designing new materials and shield configurations [5–16].

One alternative to the conventional Whipple shield is the stuffed Whipple shield. This shielding concept consists of an aluminum bumper and rear wall with intermediate layers of Nextel ceramic cloth and Kevlar fabric. In contrast to the bumper, which is impacted by a localized projectile, the intermediate cloth layers of the stuffed Whipple shield must absorb the energy of the debris cloud generated by the bumper, which is usually comprised of molten remnants of the projectile and the bumper. The cloth is more effective at absorbing diffuse debris clouds than a monolithic layer of metal, so stuffed Whipple shields are commonly employed in space applications, including on the ISS [2].

2. Metallic Glasses as Spacecraft Shields

Developing more effective Whipple shields relies on studying the effect of new materials integrated into fixed shielding geometries. Although some new shielding concepts are intended for implementation on new spacecraft architectures, as with "one-off" satellites, shielding for manned spacecraft generally requires far more rigorous verification prior to use. The overall dimensions and mass of shields, as with those used on the ISS, must typically be held constant, as launch volumes and shield masses must conform to heritage spacecraft designs [2]. As such, novel shield materials must be integrated into existing designs, which allows them to replace the bumper shield, the intermediate layer or any other configuration that maintains the overall thickness and areal density of the heritage shield. For these reasons, amorphous metals (also known as metallic glasses) are an attractive material to replace one or more of the existing shield materials in heritage configurations. In particular, metallic glasses offer a unique combination of high-hardness, high-strength, low-melting temperatures (for shield vaporization), processability similar to plastics, and moderate densities.

To date, there have been three hypervelocity investigations into the performance of metallic glasses as spacecraft shields, including two by the current authors and one by Huang et al.[17] In Davidson et al. [18], cellular structures fabricated from corrugated, welded panels of bulk metallic glass composites were tested and compared with single layers of the same materials using hypervelocity impacts of Al projectiles at 2.3 km s^{-1}, see Figure 1(a,b). This study illustrated that the debris cloud created by the bumper shield could be significantly diffused by corrugating the bumper shield's surface compared to a single-wall shield and that cellular structures created by welding the corrugated panels together could prevent penetration of the projectile with only three layers. In

Hamill et al.[19], the ballistic performance of bulk metallic glasses and bulk metallic glass composites were assessed through penetration depth experiments and penetration experiments through single-wall shields at projectile velocities ranging from 0.8 to 2.8 km s^{-1}, see Figure 1(c,d). In both of these studies, test specimens of bulk metallic glasses (BMGs) and composites based in Ti and Zr were developed specifically for the hypervelocity testing. These alloys exhibit densities that range from 5.6 to 6.0 g cm^{-3} and the purpose of the hypervelocity testing was primarily aimed at basic science results, as opposed to validating specific shielding geometries.

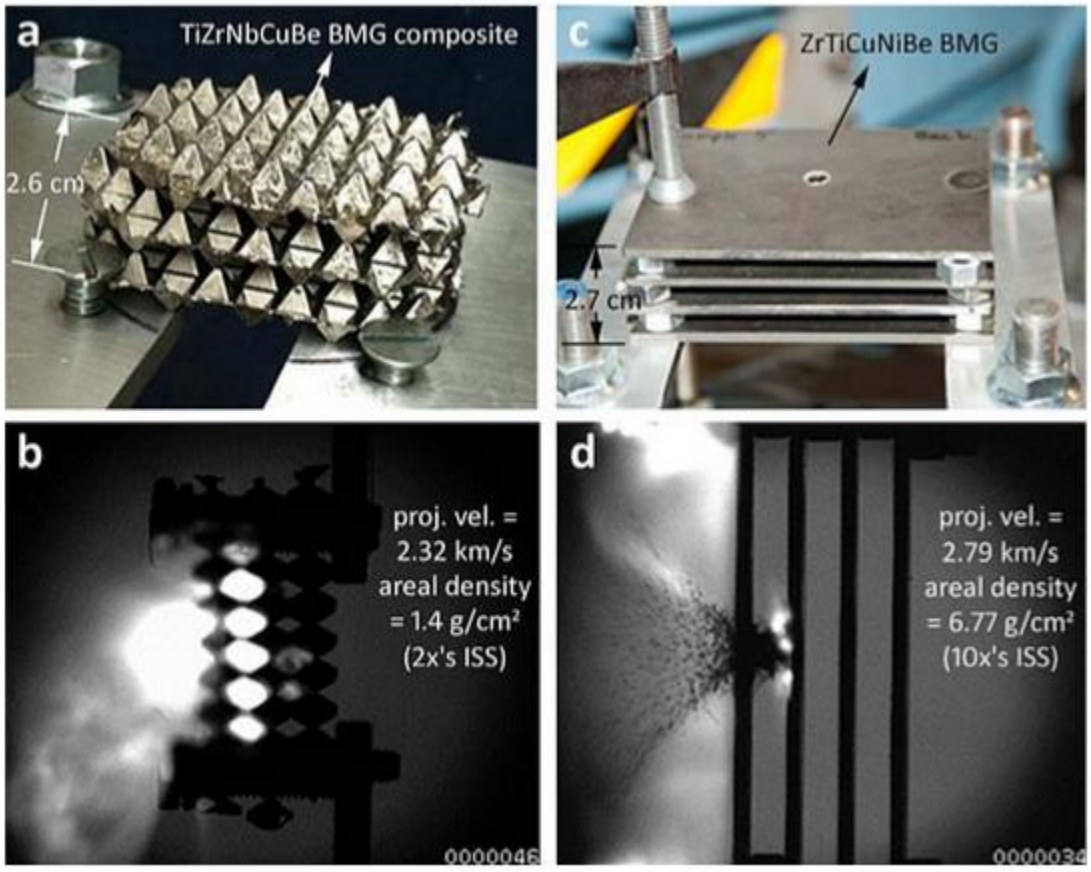

Figure 1*: (a) A three-layer Whipple shield comprised of welded layers of a Ti-based BMG matrix composite that was formed into the shape of an egg-box. (b) The shield passed a penetration test for a 3.17 mm Al projectile fired at 2.32 km s^{-1} but with double the areal density of the ISS baseline shield. (c) A four-layer Whipple shield comprised of 2.8 mm thick plates of a BMG Vitreloy 1. (d) The shield passed a penetration test for a 3.17 mm Al projectile fired at 2.79 km s^{-1} but with 10 times larger areal density than the ISS baseline shield.*

In the third study, Huang et al. [17] investigated the effect of using an Fe-Si-B metallic glass coating as the front bumper of a two-layer Whipple shield using impact velocities ranging from 3.44 to5.70 km s^{-1}, significantly faster than the other two studies. The metallic glass used in the study was applied to an LY12 Al bumper using a thermal spray coating process to create a layer 0.15 mm thick. This approach was astute because the aluminum provides a rigid substrate on which to apply the hard, metallic glass coating and the thin layer of the coating does not significantly increase the density of the bumper shield (the metallic glass used has a density of 7.2 g cm^{-3} while the Al has a density of 2.7 g cm^{-3}). As with the other two studies, the research by Huang et al. was basic science research and looked at effects such as hole size, crater morphologies, fragmentation diameter, wave propagation, and fracture surface microstructures. Although Whipple shields were tested by all three existing studies on metallic glasses, none of them were compared to heritage designs with the same areal density. The Whipple shields used in previous studies either had much higher areal densities than actual shields (3 mm thick bumpers were used in both Huang *et al*. and Hamill *et al*. while actual ISS shields have a 0.5 mm thick bumper) and the standoff distances were much larger (Ref. [17] used a 10 cm standoff while the actual ISS shield has a 2.86 cm total standoff). Figure 1 shows images from two of the BMG Whipple shields used in previous studies, Figure 1(a,b) from Ref. [18] and Figure 1(c,d) from Ref. [19]. In both, the total standoff distance is approximately equal to the baseline ISS shield used in the current study for comparison (2.86 cm), but the areal densities are higher. Figure 1(a,b) shows a three-layer BMG composite Whipple shield comprised of welded 0.8 mm thick "egg-boxes," which has an areal density of 1.4 g cm^{-2}, twice that of the baseline ISS baseline shield (0.688 g cm^{-2}). That configuration resulted in a no-penetration from the impact of a relatively slow 3.17 mm diameter Al projectile fired at 2.3 km s^{-1}. Figure 1(c,d) shows a four layer

BMG Whipple shield comprised of 2.8 mm thick plates with an areal density of 6.8 g cm^{-2}, 10 times higher than the ISS baseline. Although two layers of the BMG stopped a 3.17 mm diameter Al projectile fired at 2.79 km s^{-1}, the areal density of those two layers was still five times higher than the ISS baseline.

In the current study, the authors perform simulated orbital debris impacts in one-to-one configurations (i.e. same areal density and standoff distance) versus a one-quarter scale version of the ISS U.S. Laboratory Module cylinder shield using one of the highest velocity gun ranges available at the White Sands Testing Facility. The importance of the current experiments are twofold; (1) to test metallic glass targets under projectile velocities and diameters as similar to what would be experienced on orbit as possible and (2) to compare performance with baseline shields by keeping standoff distance and areal density constant. The kinetic energy associated with a hypervelocity impact is given by $KE = 1/2mv^2$, where *m* is the mass of the projectile and *v* is its velocity. For a spherical projectile, this can be expressed as $KE = 2/3\pi r^3 \rho v^2$, where *r* is the radius of the projectile and ρ is the density of the projectile. Kinetic energies similar to actual orbital debris strikes (8–15 km s^{-1}) can be achieved by firing larger masses at lower velocities, but this does not accurately replicate the impact physics. It is well-known in hypervelocity experiments that there are three distinct regions of behavior during impacts at different velocities. Below 5 km s^{-1}, impacts are ballistic, between 5–7 km s^{-1} melting and partial vaporization occurs, and above 7 km s^{-1} vaporization occurs. As such, there is no equivalent way of testing the performance of a shield without using a gun capable of firing at least 7 km s^{-1}.

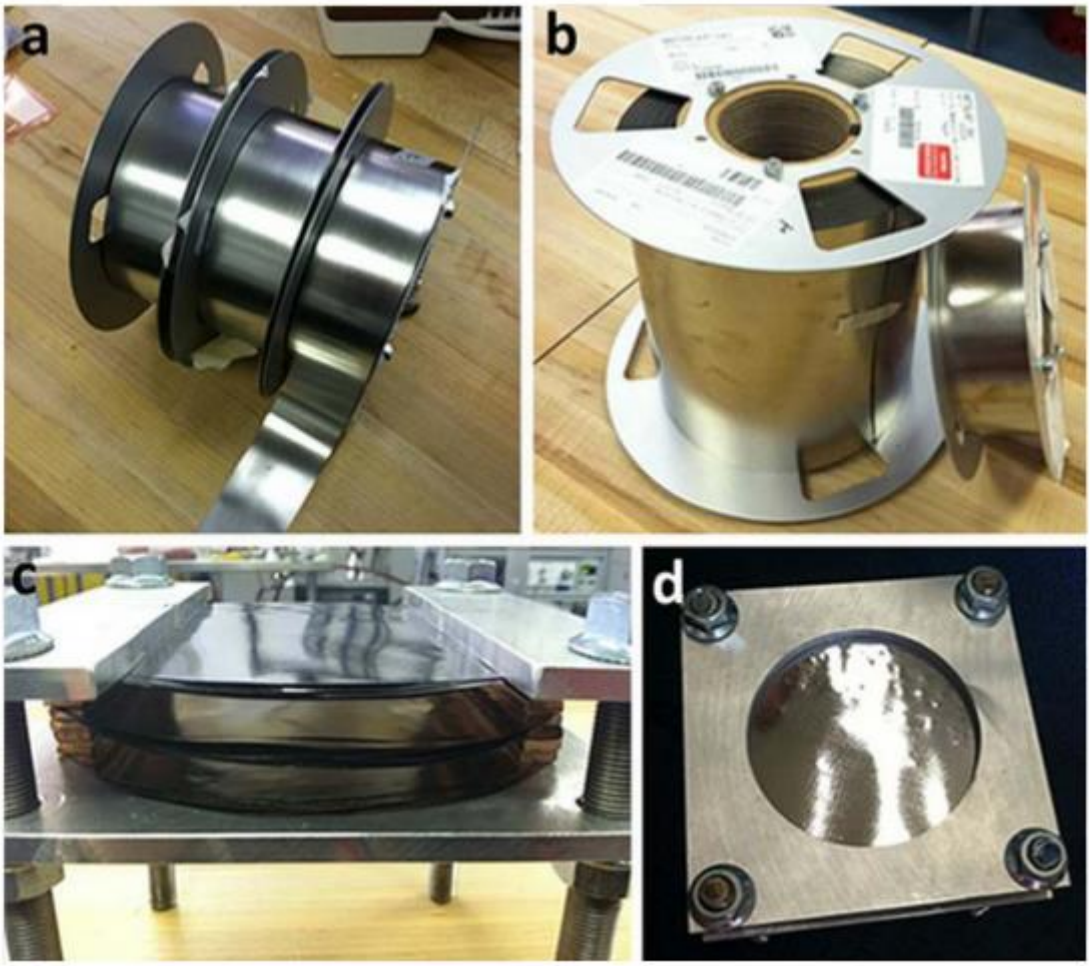

Figure 2*: (a) Rolls of 50 mm wide Fe, Ni and Co metallic glass ribbon from Allied Metglas. (b) A 21 cm wide roll of the FeSiB metallic glass ribbon used in the current experiments. (c) Example of how multiple sheets of the metallic glass from (b) can be stacked into three discrete layers of a Whipple shield within a test fixture. (d) The back side of the test fixture showing how the metallic glass layers are exposed to the target while still being confined.*

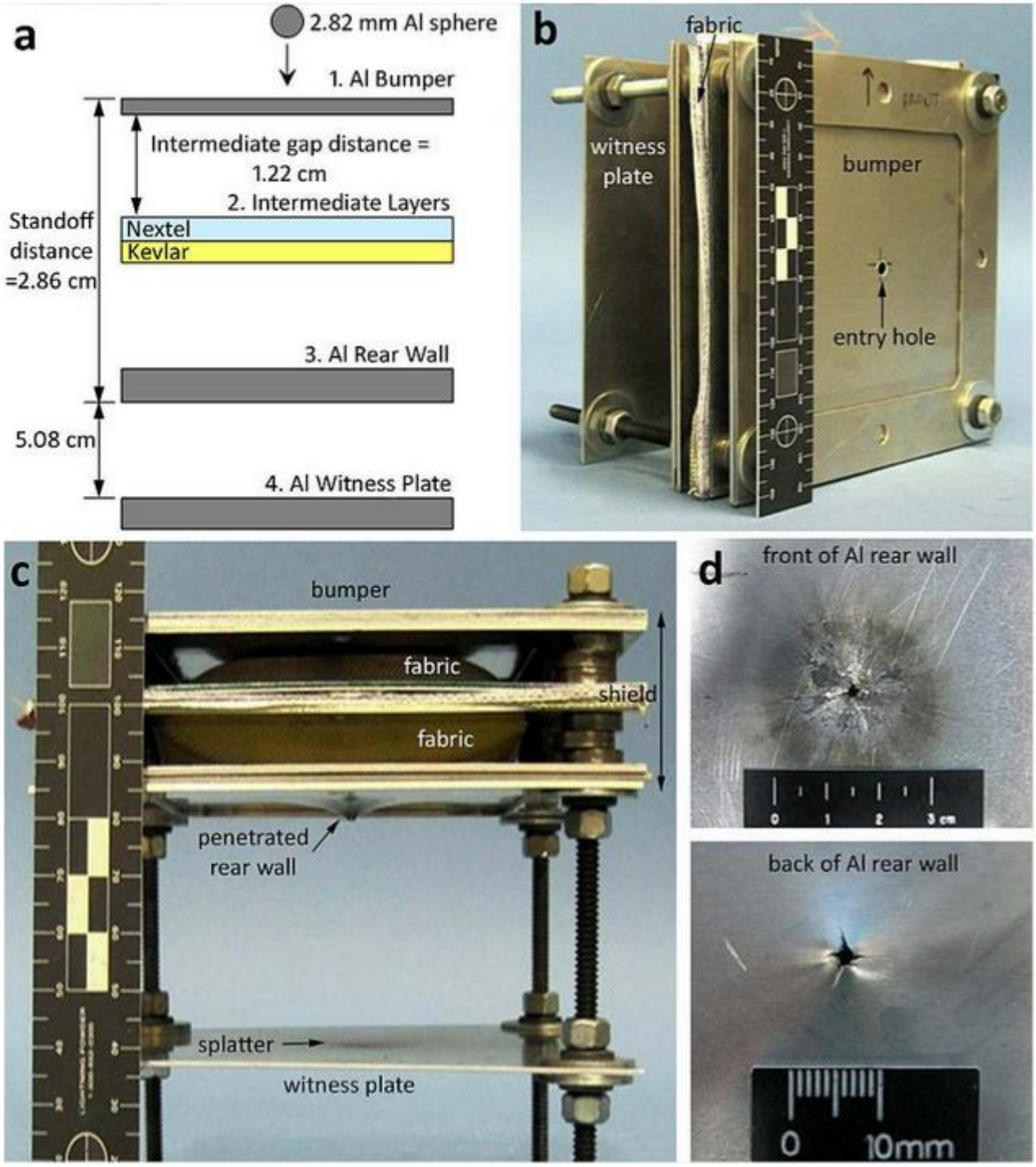

***Figure 3**: (a) Schematic of the baseline target used in the current experiments which is a 1/4 scale of the ISS U.S. Module shield. It is comprised of an Al bumper and rear wall with an intermediate layer of Nextel and Kevlar. (b) Front view of the target after penetration by the Al projectile at 6.97 km s^{-1}. (c) Side view of the target showing the penetrated rear wall and the splatter on the witness plate. (d) Front and back view of the rear wall of the shield showing total penetration.*

***Table 1**: Table 1. Three shields underwent hypervelocity impact testing with a 2.8 mm diameter aluminum sphere at 7 km s^{-1}. 'P' denotes that there was penetration of the rear wall and 'NP' denotes no penetration through the rear wall.*

Shield	Outer Bumper	Intermediate Layer	Rear Wall	Areal Density [g/cm^2]	Result
Baseline	0.5 mm Al 6061-T6	5 layers Nextel AF10 fabric 2 layers Kevlar KM2–705 fabric	1.27 mm Al 2024-T3	.688	P
1	13 layers Metglas 2605 SA1	14 layers Metglas 2605 SA1	14 layers Metglas 2605 SA1	.678	P
2	0.5 mm Al 6061-T6	11 layers Metglas 2605 SA1	1.27 mm Al 2024-T3	.675	NP

2.1. Material Preparation

The metallic glass used in the current study is a commercially available ribbon of Metglas 2605 SA1, an Fe-Si-B alloy, produced by ribbon quenching (the listed composition is $Fe_{85–95}Si_{5–10}B_{1–5}$ in weight % or $\approx Fe_{65}Si_{15}B_{20}$ in atomic %). This alloy is commonly used in the manufacture of electric transformers, due to its low cost, ease of fabrication, and excellent soft magnetic properties. However, the alloy is a weak glass former and can only be produced in amorphous ribbons up to 23 μm thick. The metallic glass has a Vickers hardness of 900, compared to 107 for Al-6061, but has 2.7 times larger density. This is a similar metallic glass to what was used by Ref. [17] as a spray coated substrate for hypervelocity testing. In the current work, 21 cm square sheets of the metallic glass ribbon were cut and then stacked together to form individual layers of the stuffed Whipple shield, while maintaining the same areal density as the actual ISS module baseline. The metallic glass sheets were tightly compressed by sandwiching them between bolted plates of Al with a cutout in the impact region. Figure 2(a,b) shows varieties of metallic glass ribbons in the as-received form from Allied Metglas. The ribbons range in thickness from 10 to 50 μm and in width from 2 to 21 cm

and are all based in Fe, Ni, or Co, as they are designed for magnetic applications (not structural). Figure 2c shows how sheets of the metallic glass ribbon can be stacked to form three layers of a hypervelocity target and Figure 2d shows how a cutout in the test fixture allows for penetration of just the metallic glass layers.

3. Hypervelocity Impact Experiments

The three hypervelocity tests as part of the current research were performed in collaboration with E. Christiansen of NASA's Johnson Space Center. Three test configurations were impacted at near-constant velocities of 6.97–7.05 km s^{-1} using a 2.8 mm diameter Al-2014 T4 sphere (impacts angles were always normal to the target).

The control target was a quarter-scale version (one-quarter of the surface area with the same standoff spacing) of the ISS U.S. Laboratory module cylinder shield using similar materials and identical configuration to the full-scale version (although the aluminum alloy and the fabric styles are slightly different in the full-scale version). The outer bumper is a 0.5 mm thick Al-6061-T6 panel with areal density of 0.138 g cm^{-2}, the intermediate materials are comprised of five layers of Nextel AF10 fabric and two layers of Kevlar KM2–705 fabric with a total areal density of 0.195 g cm^{-2}, and the rear wall is a 1.27 mm thick Al 2024-T3 panel with areal density of 0.355 g cm^{-2}. The total areal density of the target was 0.688 g cm^{-2}. An intermediate gap distance of 1.22 cm was used between the bumper and the fabric, and the total standoff distance of the shield was 2.86 cm. An Al 2024-T3 witness plate 1.0 mm thick was spaced 5.08 cm behind the rear wall to collect splatter.

The first test target was assembled of all metallic glass sheets in three distinct layers. The bumper was comprised of 13 stacked sheets of Metglas 2605 SA1 with areal density of 0.215 g cm^{-2}, the

intermediate layer was 14 stacked sheets of the same metallic glass with areal density of 0.232 g cm^{-2}, and the rear wall was also 14 stacked metallic glass sheets. The total areal density of the metallic glass target was 0.678 g cm^{-2}, which is just slightly lower than the baseline target. The overall standoff of the metallic glass shield was 2.86 cm, which was identical to the baseline target.

The second test target was comprised of an identical setup as the baseline target except the fabric layers were replaced with 11 sheets of Metglas 2605 SA1 with an areal density of 0.182 g cm^{-2}. The total areal density of the target was 0.675 c cm^{-2} (less than the baseline) and the overall standoff distance was maintained at 2.86 cm.

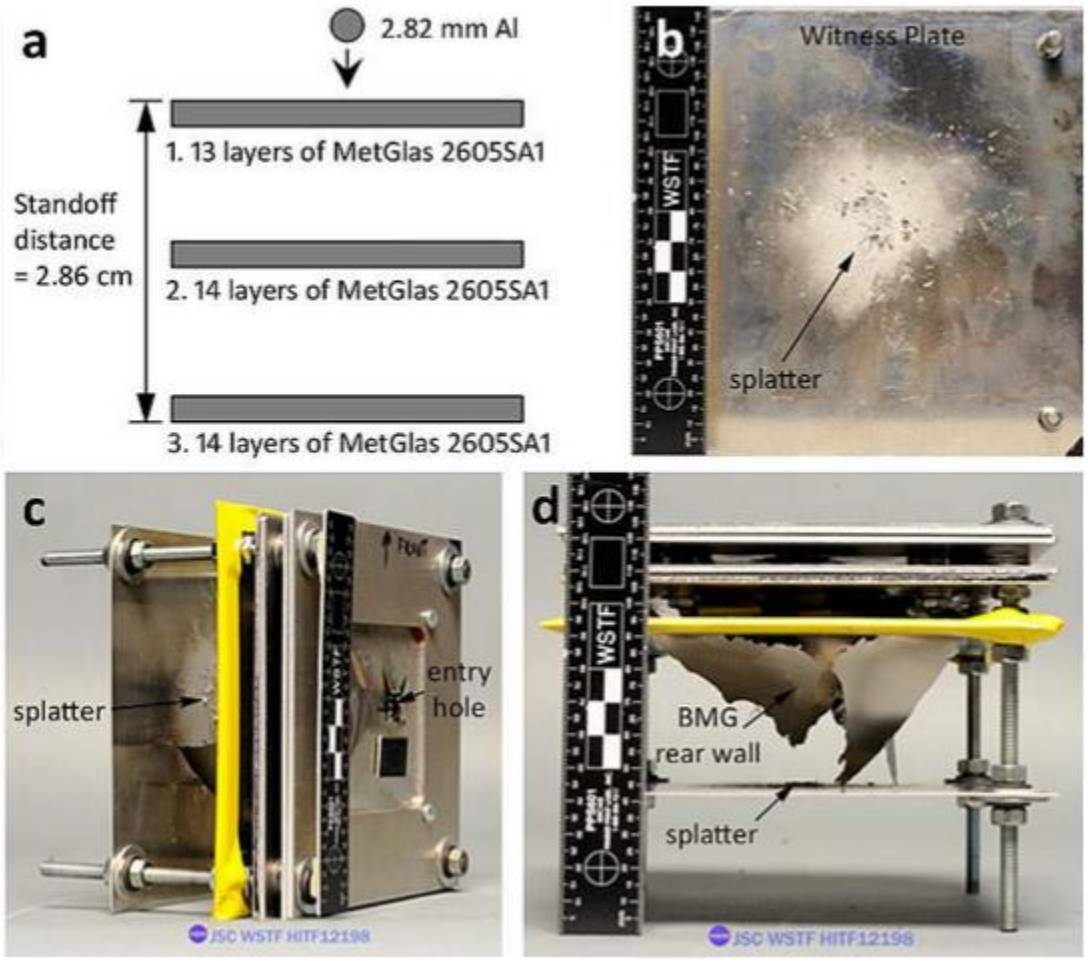

***Figure 4**: (a) Schematic of a test sample with all three layers of the shield comprised of stacked sheets of an FeSiB metallic glass. (b) Splatter on the witness plate after complete perforation of the shield from an Al projectile fired at 7.05 km s^{-1}. (c) Front view of the target showing large entry hole and debris on witness plate. (d) Side view of the target showing massive tearing of the metallic glass rear wall.*

4. Results

Table 1 shows the results of the three hypervelocity experiments, one on the baseline target and two on the metallic glass targets. The baseline target failed by perforation from the impact of the 0.032 g Al projectile at 6.97 km s^{-1} creating a 2.1 by 1.8 mm hole in the rear wall, shown in Figure 3. The witness plate was splattered with debris but was not penetrated or bulged, see Figure 3c. The quarter-sized shield with similar materials to the ISS module shield was therefore inadequate to prevent

perforation by the Al projectile in that configuration. It should be noted that the boundary effects of the propagating wave may cause the full size version to behave differently, but this was not investigated. Figure 3a shows a schematic of the baseline target, Figure 3(b,c) show a front view and a side view, respectively, of the target after impact and Figure 3d shows the hole in the front and back of the Al rear wall.

The first test target, comprised of three layers of stacked metallic glass sheets, also failed from the impact of a 0.032 g Al projectile at 7.05 km s^{-1}, creating a large hole in the rear wall, shown in Figure 4. The witness plate was splattered with debris, Figure 4b and the rear wall of the shield experienced a large amount of tearing, a result of the low toughness of the metallic glass alloy, see Figure 4d.

The third test target, where the metallic glass sheets replaced the Nextel and Kevlar fabrics, passed the test by not being penetrated by the 0.032 g Al projectile at 6.97 km s^{-1}, see Figure 5. The Al 2024-T3 rear wall was bulged by the impact but did not experience penetration, perforation, or detached spall, resulting in a pass. Figure 5(d,e) show front and side view images of the target just before impact, where the Al projectile can be seen in both images. Figure 5(f,g) are images taken 0.1 ms after triggering the camera, showing vapor and fragment clouds in the front view and a debris cloud creating a bulge in the rear wall in the side view.

5. Analysis and Discussion

Figure 5 shows that the main result of the current set of hypervelocity experiments is that the target with the metallic glass layers replacing the Nextel and Kevlar fabrics was not penetrated during impact, while the heritage shield with similar characteristics to the ISS shield and the all-metallic glass shields were. In itself, this is an impressive result because one shield configuration comprised

of metallic glass passed the test. It is also very surprising because it is counterintuitive that the metallic glass layers, which are hard and brittle, would perform better than the energy-absorbing fabric at preventing penetration of the rear wall.

The side-view image of the target that passed (Figure 5g) shows qualitatively why the metallic glass intermediate layer behaved better than the fabric at preventing penetration of the rear wall. The entry hole into the Al bumper is just larger than the Al projectile (Figure 5(b,f)) and yet the exit hole from the intermediate layer of metallic glass sheets is distributed over several centimeters of area, leading to a bulging of the Al-rear wall that is over a centimeter in diameter. In contrast, the ISS analogue shield had a 2.1 by 1.8 mm diameter hole in the rear wall, indicating that neither the bumper nor the fabric was able to diffuse the cross-sectional impact area of the debris enough to prevent penetration of the Al rear wall.

Figure 6 describes the formation and propagation of the bulge that was created in the Al rear wall from test that passed, shown in Figure 5. The data from Figure 6 were taken in the first 0.5 ms after the Al projectile triggered the laser, where impact into the bumper occurred approximately 90 μs after the trigger. In the second frame captured by the high-speed camera (0.1 ms after the trigger), shown in Figure 5g, the projectile and debris has already passed through the bumper, the metallic glass intermediate layer and has created a small bulge in the rear wall. The total transit time from the projectile impacting the bumper to the debris impacting the rear wall is estimated to be only 15 μs. The depth of the bulge, as referenced from the flat rear wall prior to impact, was measured from each frame of the impact data and is plotted in Figure 6a. The bugle initially grows very fast, reaches a plateau at approximately 5 mm deep, and then has a ringing oscillation around this value until

damping occurs. The growth of the bulge to the steady-state depth is fit by the sixth order polynomial equation:

$$d = -16010t^6 + 37169t^5 - 34417t^4 + 16352t^3 - 4225.5t^2 + 567.14t - 26.323, \quad (1)$$

where d is the depth of the bulge in millimeters and t is the time delay from the triggering of the laser in milliseconds. The data show that the bulge reaches its maximum deflection approximately 100 μs after the initial impact. Figure 6b shows the width of the bulge as measured from the side-view for the first 0.5 ms after the laser trigger. The width of the bulge initially propagates as a wave, spanning the entire sample before damping to approximately 30 mm wide, and then ringing about this value for the remainder of the video. The wave propagation in the rear wall can be seen visually in Figure 6c by taking a linescan of the rear wall after the impact. The damage to the rear wall is detailed in Figure 6 primarily for two reasons; (1) to show the extent of damage that the outer wall of the spacecraft may incur during this type of impact and (2) to show the propagation of the wave through the rear wall, which demonstrates that there are clearly boundary effects in the testing setup which may influence the performance of the shield compared to a full sized version. Tiled images from the video are compiled and shown in Figure 7 for the side view of the impact.

For the target that passed the test, it is unclear exactly what the mechanism was that allowed the intermediate layer of metallic glass to diffuse the debris cloud. It is possible, as Huang et al. argued that the increased hardness of the metallic glass completely melts the projectile and the liquid phase has less penetrating power than the solid phase[17]. However, one effect that cannot be discounted in the current set of experiments is that the stacked layers of metallic glass were not actually rigid, which may have allowed them to diffuse impact energy laterally between each layer. It is, therefore,

unclear if a 0.25 mm thick monolithic plate of metallic glass would perform similarly to the 11 stacked layers of 23 μm thick ribbon; however, Metglas 2605 SA1 cannot be fabricated in free-standing panels of this thickness, due to its limited glass-forming ability.

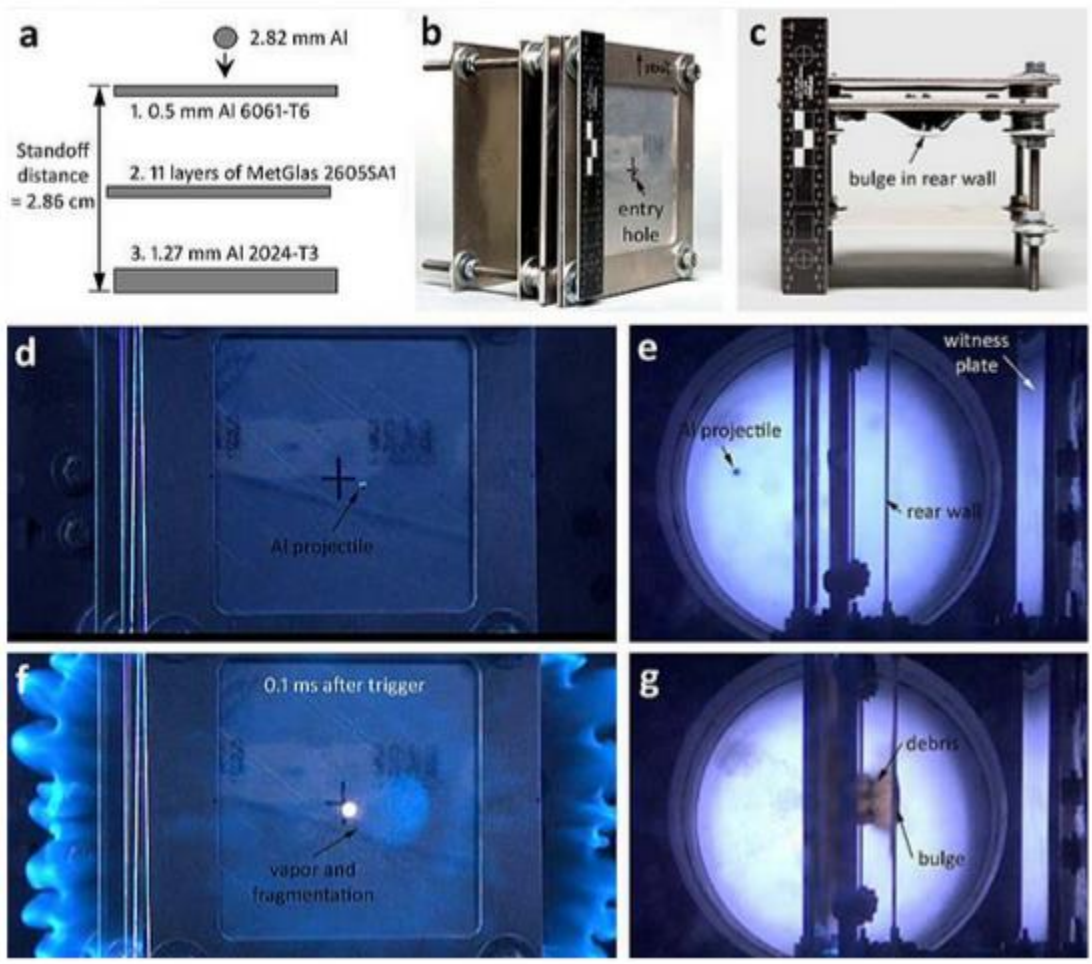

***Figure 5**: (a) Schematic of the target that passed the test, showing the layers of metallic glass that replaced the fabric layers in the baseline target. (b) Front view of the target showing the entry hole from the Al projectile fired at 6.97 km s^{-1}. (c) Side view of the target showing a bugle in the rear wall but no perforation. (d) A frame from the high-speed camera 81 ms after the projectile triggered the laser and (e) side view of the target just prior to impact. (f) Front view of the target 106 ms after triggering the laser and approximately 15 ms after impact showing vapor and fragmentation. (g) Side view of the target showing that debris has already deformed the rear wall in the second frame captured by the camera.*

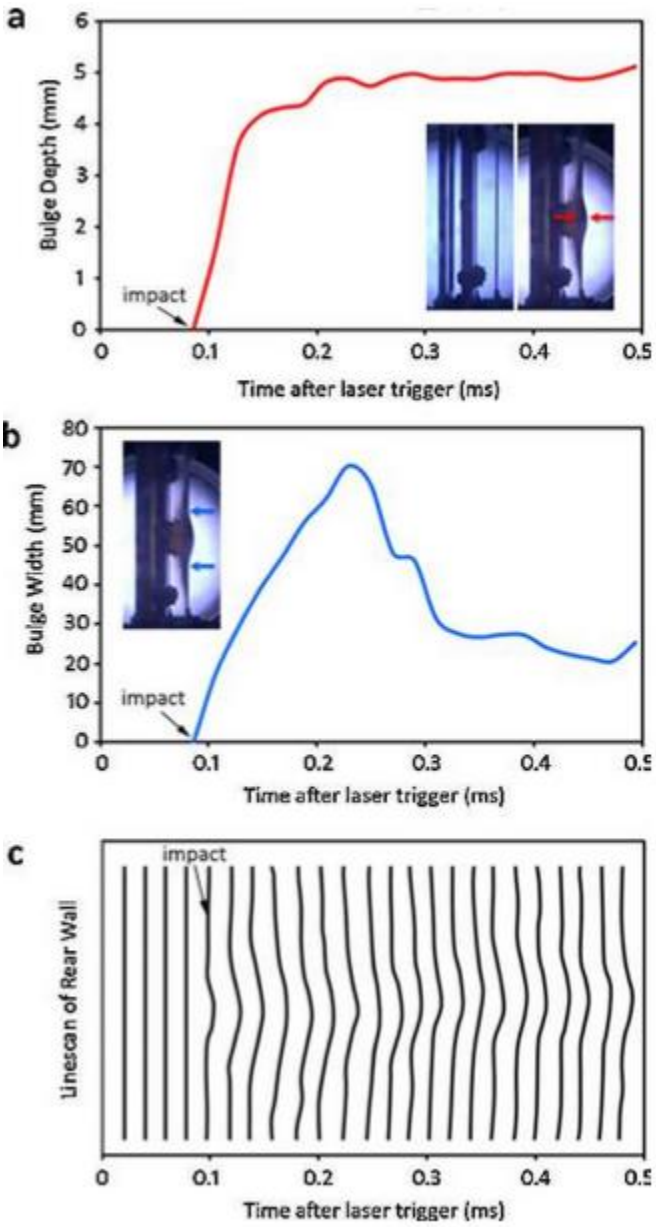

***Figure 6**: (a) Plot of the depth of the bulge in the rear wall of the target from Figure 5 measured from frames in the high-speed video for the first 0.5 ms after the laser triggering. The bulge rapid grows to approximately 5 mm and oscillates about this value. (b) Plot of the width of the bulge as a function of time showing the initial wave propagation of the rear wall after impact. This can be seen visually in (c) by viewing a linescan of the rear wall over the same 0.5 ms.*

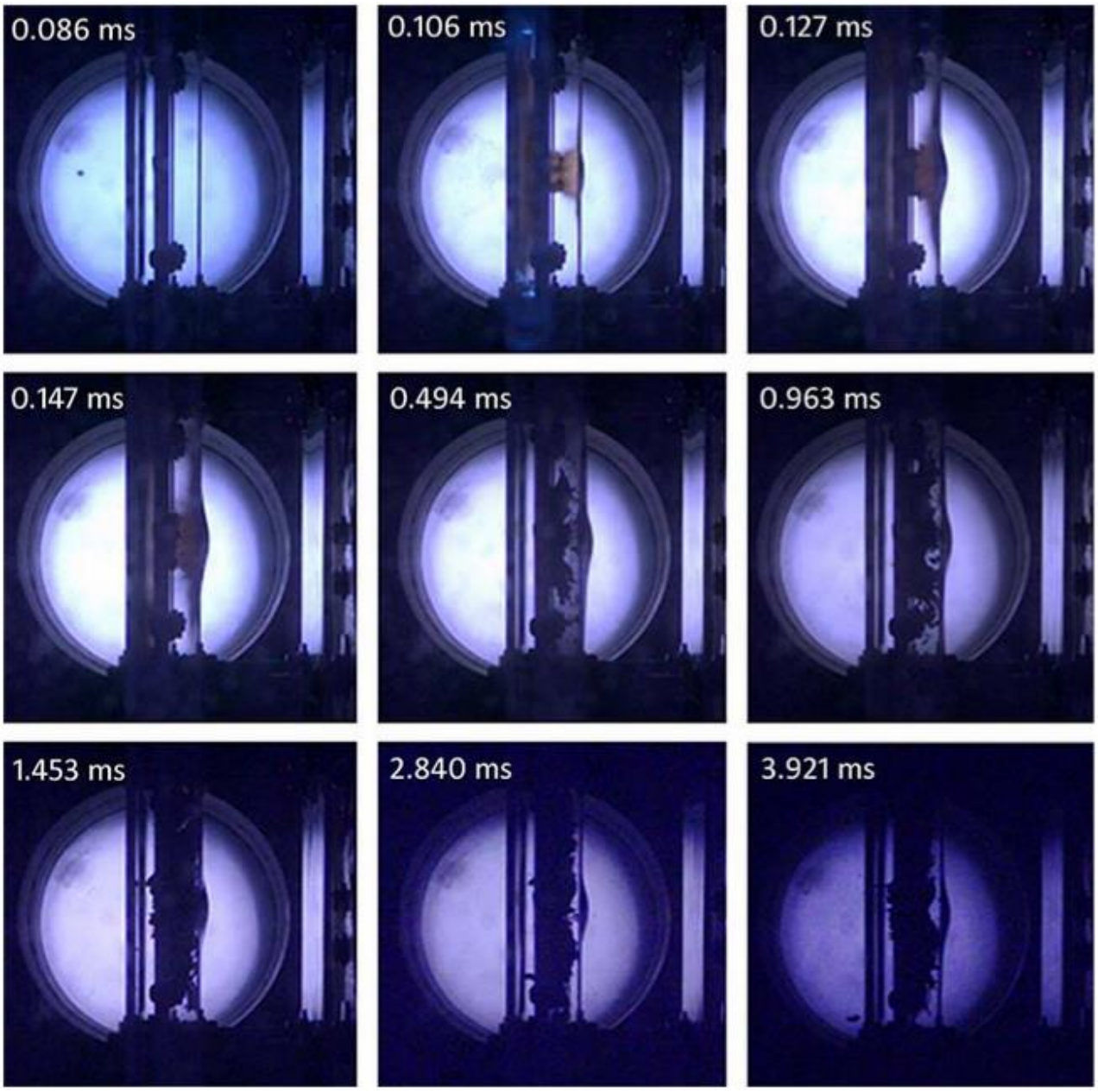

***Figure 7**: Frames from the hypervelocity impact into the target with metallic glass intermediate layers at various times up to 4 ms after impact. The rear wall is seen to bulge but is not perforated by the debris cloud, resulting in a test pass.*

6. Future Directions

The four hypervelocity studies to date on metallic glasses as potential spacecraft shielding have provided important data about which features of these novel materials are suitable for spacecraft implementation. As predicted by ballistic limit equations (see Ref. [18]), the major benefits of metallic glasses in shields are hardness, ability to be formed into corrugated structures or cellular structures (for diffusing impacts), low melting points (to assure complete melting during impact), and low densities (in some alloys). Based on the four existing studies, it is conceivable that metallic glasses could be utilized in existing architectures, where density and standoff distances are fixed, or they could be used in new shield concepts for future spacecraft or satellites, such as cellular structures or foams.

It is likely that future work on integrating metallic glasses into spacecraft shields will take threeforms; (1) developing new alloys that have optimal combinations of hardness and density, (2) designing shield architectures that best exploit the advantageous properties of metallic glass, and (3) developing new manufacturing processes to fabricate the metallic glass shields.

Based on a survey of the literature, there are many metallic glass alloys that exhibit a lower density than the alloys that have been used in the current (and previous) studies on BMG shields [20]. Low-density metallic glasses have been developed in Al-based systems (2.8–3.6 g cm^{-3}), Mg-based systems (2.6–4.2 g cm-3), Ca-based systems (1.9–2.6 g cm^{-3}), and Ti-based systems (4.5-7.2g cm^{-3}) [20]. Of these, Al and Ti-based metallic glasses have the most promise, due to the extremely low-density of the Al alloys and the high toughness of the Ti alloys (the Ca and Mg metallic glasses are exceptionally brittle). Only two BMGs have been developed in Al systems, $Al_{86}Si_{0.5}Ni_{4.06}Co_{2.94}Y_6Sc_{0.5}$ and $Al_{86}Y_{4.5}Ni_7Co_1La_{1.5}$, and these alloys have a moderate Vicker's

hardness of approximately 300. Ti-based BMGs, such as $Ti_{45}Zr_{20}Be_{35}$, have low density (<5 g cm^{-3}) but also can have high hardness (>600 Vicker's). Some of these alloys can be formed as bulk glasses in dimensions up to 5 cm thick and typically have excellent fracture toughness (50–80 MPa $m^{1/2}$).

Once an optimal metallic glass alloy is selected, there are a variety of ways to integrate it into a spacecraft shield. These include (1) applying the metallic glass as a spray coating on an existing shield, (2) using it as a layer in a Whipple shield, (3) using it as a cellular structure, and (4) using it as a stochastic foam. Previous literature has already explored the possibilities of using metallic glass in each of these configurations as energy-absorbing structures but future work will require extensive modeling and simulation to predict the optimal geometries for each type of spacecraft [21–23].

The largest current limitation in the application of metallic glasses in spacecraft shields is fabrication. To be used efficiently in spacecraft, metallic glasses need to be easily produced as thin panels (0.2–1 mm thick) with large surface area, coatings with uniform properties and tailorable compositions, stochastic foams with large surfaces areas and complex cellular structures (such as honeycombs). Of these manufacturing technologies, the fabrication of thin panels is the most desirable, considering that these could be used as freestanding shields, combined into laminates, or formed in a post-processing step into cellular structures. Unfortunately, panels of metallic glass cannot easily be fabricated above 0.1 mm thick and below 1 mm thick. Ribbon quenching is used to fabricate thin metallic glass sheets such as the ones used in the current study, but this technology cannot be used for ribbons above 0.1 mm in thickness. In contrast, die-casting can only be used to make panels >1 mm in thickness, due to the liquid front freezing in thin molds. Much effort has been spent in developing new manufacturing technologies, such as twin-roll casting, to develop sheet-

metal out of metallic glasses. Ultimately, these new alloys and architectures will finally allow full-scale metallic glass shields to be built and qualified.

7. Conclusion

Although the number of impact shots available for the current study was small, a compelling case is made for using metallic glasses as an intermediate layer in spacecraft stuffed Whipple shields. When tested under identical conditions with a baseline Whipple shield similar to what is currently used on the ISS, a shield with intermediate layers of metallic glass passed the test while the baseline sample did not. The results from the current set of experiments, in combination with similar previous studies, is then used to suggest future alloys and shield geometries which may improve the performance of metallic glasses in hypervelocity impacts, ultimately leading to their implementation.

References:

1. R. P. Bernhard, E. L. Christiansen, D. E. Kessler, Int. J. Impact Eng. 1997, 20, 111.
2. E. L. Christiansen, K. Nagy, D. M. Lear, T. G. Prior, Acta Astron. 2009, 65, 921.
3. E. L. Christiansen, AIAA/NASA/DOD Orbital Debris Conference: Technical Issues & Future Directions 1990.
4. *Orbital Debris, A Technical Assessment*, National Academy Press, Washington, D.C. 1995.
5. E. L. Christiansen, J. H. Kerr, Int. J. Impact Eng. 1997, 20, 165.
6. A. J. Piekutowski, K. L. Poormon, E. L. Christiansen, B. A. Davis, Int. J. Impact Eng. 2011, 38, 495.
7. S. Ryan, M. Bjorkman, E. L. Christiansen, Int. J. Impact Eng. 2011, 38, 504.
8. E. L. Christiansen, J. H. Kerr, Int. J. Impact Eng. 2001, 26, 93.
9. J. H. Robinson, A. M. Nolen, Int. J. Impact Eng. 1995, 17, 685.
10. C. J. Hayhurst, I. H.G. Linginstone, R. A. Clegg, R. Destefanis, M. Faraud, Int. J. Impact Eng. 2001, 26, 309.
11. E. A. Taylor, M. K. Herbert, B. A. M. Vaughn, J. A. M. McDonnell, Int. J. Impact Eng. 1999, 23, 883.
12. J.-M. Sibeaud, L. Thamie, C. Puillet, Int. J. Impact Eng.2008, 35, 1799.
13. W. Schonberg, F. Schafer, R. Putzar, Acta Astron. 2010, 66, 455.

14. M. Grujicic, B. Pandurangan, C. L. Zhao, S. B. Biggers, D. R. Morgan, App. Sur. Sci. 2006, 252, 5035.
15. W. P. Schonberg, Adv. Space Res. 2010, 45, 709.
16. R. Destefanis, F. Schafer, M. Lambert, M. Faraud, Int. J. Impact Eng. 2006, 33, 219.
17. X. Huang, Z. Ling, Z. D. Liu, H. S. Zhang, L. H. Dai, Int. J. Impact Eng. 2012, 42, 1.
18. M. Davidson, S. Roberts, G. Castro, R. P. Dillon, A. Kunz, H. Kozachkov, M. D. Demetriou, W. L. Johnson, S. Nutt, D. C. Hofmann, Adv. Eng. Mat. 2012, 15, 27.
19. L. Hamill, S. Roberts, M. Davidson, W. L. Johnson, S. Nutt, D. C. Hofmann, Adv. Eng. Mat. 2013, 16, 1.
20. J.-Z. Jian, D. C. Hofmann, D. J. Jarvis, H.-J. Fecht, Adv. Eng. Mater. 2014, 10.1002/adem201400252 .
21. M. Demetriou, C. Veazey, J. Harmon, J. Schramm, W. Johnson, Phys. Rev. Lett. 2008, 101, 145702.
22. D. C. Hofmann, H. Kozachkov, H. Khalifa, J. Schramm, M. Demetriou, K. Vecchio, W. Johnson, JOM 2009, 61, 11.
23. J. Schramm, D. C. Hofmann, M. Demetriou, W. Johnson, Appl. Phys. Lett. 2010, 97, 24.